THE MECHANICS OF MULTIPLE TRANSVERSE CRACKING IN COMPOSITE LAMINATES

J. R. YEH

Aluminum Company of America, Alcoa Laboratories, Alcoa Center, PA 15069, U.S.A.

Abstract—Fracture mechanisms of multiple transverse cracking in composite laminates are examined by using a finite element method employing special singular elements. Since these special elements contain the exact stress singularity, the stress intensity factors and energy release rates at the crack tip can be determined conveniently with a high degree of accuracy and a fast rate of convergence. In this paper, the critical conditions for the behavior of multiple transverse cracking are studied analytically on the basis of fracture mechanics theory. The numerical predictions are compared with experimental results for [0/90], laminates of various thicknesses. Very close agreement is obtained.

1. INTRODUCTION

Damage due to multiple transverse cracks has been observed in experiments on fibrous composite laminates by Parvizi and Bailey (1978), Highsmith and Reifsnider (1982) and Crossman *et al.* (1980). In general, these cracks occur primarily in plies whose fibres are oriented transverse to the applied load. Laminate property degradation due to these cracks is detrimental to structure reliability.

Theoretical studies of the initial stage of transverse cracking have been conducted by Bailey *et al.* (1979), Wang, A. and Crossman (1980) and Dvorak and Laws (1987). As the applied load increases, subsequent cracks in the laminate are formed. At this stage, the interaction of cracks must be considered. A multiple cracking theory based on shear lag analysis was developed by Parvizi and Bailey (1978). In their analysis, a one-dimensional model based on a strength of materials formulation was used. Interaction of cracks was not included in their model.

Finite element analysis incorporating the virtual crack closure technique was conducted by Wang, A. (Wang, A. and Crossman, 1980; Wang, A., 1984). In his paper, the crack interaction was included, and it has been demonstrated that the energy release rate concept as a criterion for crack growth can be used in the failure analysis of composite laminates. However, the accuracy of the technique has been a subject of concern. Since the stress field near the crack tip is singular, the traditional finite element approach requires too many elements. In this paper, special singular elements containing the exact stress singularity are used. The energy release rate at the crack tip can be determined conveniently with a high degree of accuracy and a fast rate of convergence.

In the next section, the fundamental nature of the interface tip stress singularity of a transverse crack in [0/90], laminate is examined. A finite element method employing special singular elements, which contain the exact stress singularity, is presented in Section 3. By using this method, the stress intensity factors and energy release rates for each mode can be determined. In Section 4, the critical energy release rate is obtained by interpreting the experimental results. The critical energy release rate is compared with the results of Section 3 to determine the critical applied stress for flaw growth with given crack spacing in Section 5. Finally, numerical examples for [0/90], laminates with various thicknesses are studied and discussed in Section 6.

2. INTERFACE TIP STRESS SINGULARITY OF TRANSVERSE CRACK IN [0/90], LAMINATE

When a crack is embedded in a medium, the order of the stress singularity at the crack tip is -0.5. If the crack is terminated at an interface of two media, the stress singularity

Table 1. Material properties of the glass epoxy composite

E_1 (GPa)	E_2 (GPa)	G_{12} (GPa)	G_{23} (GPa)	v_{12}	v_{23}	x_1 (10^{-6} per °C)	x_2 (10^{-6} per °C)
42	14	5	5	0.27	0.27	4.3	14.3

The subscripts 1, 2 and 3 denote the fiber, transverse and thickness directions of the glass/epoxy composite, respectively.

order is no longer -0.5. By solving the pertinent eigenvalue problem, the stress singularities, δ_n, at the interface tip of the crack can be determined. Recently, this problem has been solved analytically by Ting and Chou (1981), Zwiers *et al.* (1982) and Wang, S. and Choi (1982), and numerically by Yeh and Tadjbakhsh (1986). For the glass/epoxy composite listed in Table 1, there exist three orders of interface tip stress singularities of the crack normal to 0-90 ply interface. The resulting orders of the singularities are:

$$\delta_I = -0.423$$

$$\delta_{II} = -0.500$$

$$\delta_{III} = -0.500. \qquad (1)$$

For every eigenvalue, δ, there exists a corresponding eigenvector, which represents the possible mode of deformation around the crack tip. The modes of deformation for the crack in a [0/90] laminate are shown in Fig. 1. The loading case considered in this study is dominated by the opening mode of deformation, and the stress singularity, δ_I, is used in the analysis.

3. PROBLEM FORMULATION

Consider a [0/90], laminate, which has a transverse ply thickness $2d$ and a longitudinal ply thickness b as shown schematically in Fig. 2. When the laminate is subjected to a
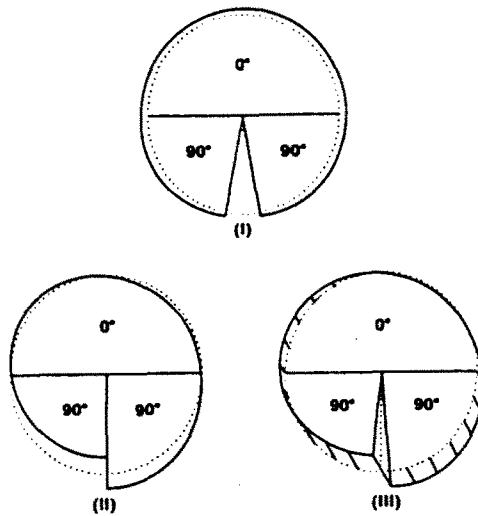

Fig. 1. The modes of deformation for the transverse crack in [0/90] laminate. (I) opening mode, (II) shear mode, and (III) tearing mode.
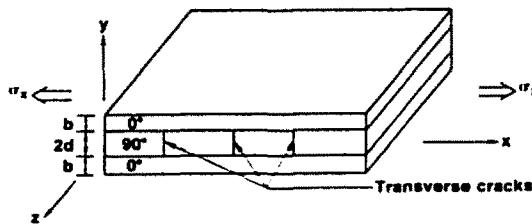

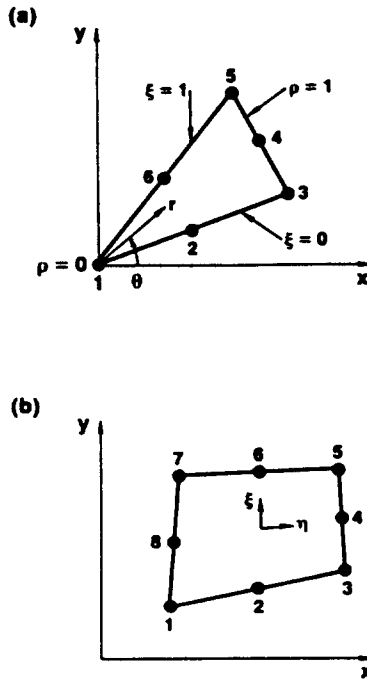Fig. 2. Geometry of multiple transverse cracks in [0/90], laminate.

Fig. 3. (a) Six-node singular element and (b) eight-node isoparametric element.

sufficiently large tensile stress in the x-direction (0"), the transverse ply may suffer multiple cracks such as illustrated in the figure. This problem is treated as a generalized plane strain problem (Lekhnitskii, 1963). The components of displacement are assumed to be independent of the z-direction, and the laminate is subjected to a constant strain, ε_0, in the z-direction such that the total force in the z-direction is equal to zero.

Owing to the singular nature of the transverse cracks in composite laminates, the special numerical method employing conforming singular finite elements is an attractive approach to the current problem. In this approach, the exact stress singularity at the crack tip can be included in the formulation of the special elements. The concept of the conforming singular element was originally introduced by Stern (1979), and has been applied to problems of an interlaminar delamination in fiber-reinforced composite materials by Wang, S. and Choi (1984) and Yeh (1988). Detailed discussion of the nature of the singular elements was given in Yeh (1988). Only relationships relevant to the current problem are presented here.

Consider a six-node triangle element with three degrees of freedom per node and the stress singularity at the node 1 as shown in Fig. 3a. By a proper transformation, any point in the element defined in global Cartesian coordinates (x, y, z) can be referred to both polar coordinates (r, θ, z) and local triangular coordinates (ρ, ξ, z) with the origin located at node 1. Within the element, the displacements, $\{U\}$, are related to the nodal displacements, $\{q\}$, by the shape function, $[N_s]$ and the constant strain, ε_0, as

$$\{U\} = [N_s]\{q\} + \{U_0\} \tag{2}$$

where

$$\{U\}^T = \{u, v, w\}$$

$$\{q\}^T = \{u_1, v_1, w_1, \ldots, u_6, v_6, w_6\}$$

$$[N_s] = [N_s(\rho, \xi; \delta)]$$

$$\{U_0\}^T = \{0, 0, \varepsilon_0 z\}. \tag{3}$$

Explicit expressions of the shape function involving the proper stress singularity order, δ, and local coordinates, (ρ, ξ), are given in the Appendix. Excluding the rigid body motion, then eqn (2) can be rewritten in a more explicit form as follows:

$$\{U\} = \{\rho^{\delta+1}[M(\xi)] + \rho[L(\xi)]\}\{q\} \tag{4}$$

where $[L(\xi)]$, $[M(\xi)]$ are the nonsingular and singular parts of $[N_s(\rho, \xi; \delta)]$, respectively. The ρ and ξ are related to the global coordinates by the simple transformation given in the Appendix.

The surrounding nonsingular elements used in this study are quasi-three-dimensional eight-node isoparametric elements (Fig. 3b) with 24 degrees of freedom. The shape function of the singular element is chosen such that the element conforms with a nonsingular quadratic element at the common element boundary (i.e. along edge 3–5), and with singular elements of the same formulation along boundaries 1–3 and 1–5.

In a manner consistent with the interface crack between dissimilar isotropic media (Comninou, 1977), the delamination stress intensity factors are defined as follows:

$$K_1 = \lim_{r \to 0} \sqrt{2\pi} r^{-\delta} \sigma_x(r, \pi/2)$$

$$K_{II} = \lim_{r \to 0} \sqrt{2\pi} r^{-\delta} \tau_{xy}(r, \pi/2)$$

$$K_{III} = \lim_{r \to 0} \sqrt{2\pi} r^{-\delta} \tau_{xz}(r, \pi/2). \tag{5}$$

The energy release rates may be evaluated by using the virtual crack extension concept (Irwin, 1957):

$$G_1 = \lim_{c \to 0} \frac{1}{2c} \int_0^c \sigma_x(r, 0)\,[u(c-r, -\pi/2) - u(c-r, 3\pi/2)]\,dr$$

$$G_{II} = \lim_{c \to 0} \frac{1}{2c} \int_0^c \tau_{xy}(r, 0)\,[v(c-r, -\pi/2) - v(c-r, 3\pi/2)]\,dr$$

$$G_{III} = \lim_{c \to 0} \frac{1}{2c} \int_0^c \tau_{xz}(r, 0)\,[w(c-r, -\pi/2) - w(c-r, 3\pi/2)]\,dr \tag{6}$$

where c is the length of virtual crack extension. It can be seen that the stress intensity factors and energy release rates at the crack tip can be evaluated from the asymptotic solutions of stress and displacement along the plane of the crack.

The asymptotic stress and displacement can be conveniently determined by this singular finite element method. Along the crack plane, $\xi = \theta_0$, the stress and displacement fields near the crack tip can be approximated by using eqn (4) and its derivatives as:

$$\{\sigma\} = \rho^\delta[P(\theta_0)]\{q\} \tag{7}$$

$$\{U\} = \rho^{\delta+1}[M(\theta_0)]\{q\} \tag{8}$$

where $[P(\theta_0)]$ is a product of the stiffness matrix and the matrix of derivatives of the shape function $[M(\xi)]$. For $\{\sigma\}$ and $\{U\}$ along the crack plane $\theta_0 = \pi/2$, the asymptotic stresses and displacements can be written as follows:

$$\sigma_x = A_1 r^\delta, \quad \tau_{xy} = A_{II} r^\delta, \quad \tau_{xz} = A_{III} r^\delta, \tag{9}$$

$$u = B_1 r^{\delta+1}, \quad v = B_{II} r^{\delta+1}, \quad w = B_{III} r^{\delta+1}, \tag{10}$$

where

$$B_i = B_{i-}^+ - B_i^- \quad \text{for } i = \text{I, II, III} \tag{11}$$

in which the A_i's, B_i^+'s and B_i^-'s are obtained from the corresponding components of $[P(\pi/2)]$, $[M(-\pi/2)]$ and $[M(3\pi/2)]$ in eqns (7) and (8). Thus, the stress intensity factors K_i can be easily determined from eqn (5):

$$K_i = \sqrt{2\pi} A_i \quad \text{for } i = \text{I, II, III.} \tag{12}$$

The energy release rates can be determined through eqn (6) as:

$$G_i = \lim_{c \to 0} \frac{1}{2c} \int_0^c (A_i r^\delta)[B_i(c-r)^{\delta+1}] \, dr$$

$$= \frac{A_i B_i}{2} \beta(2+\delta, 1+\delta) \lim_{c \to 0} c^{1+2\delta} \quad \text{for } i = \text{I, II, III} \tag{13}$$

where β is the Beta function as defined in Gradshteyn and Ryzhik (1980). For the inverse square root singularity, eqn (13) becomes:

$$G_i = \frac{\pi}{4} A_i B_i \quad \text{for } i = \text{I, II, III.} \tag{14}$$

4. CRITICAL ENERGY RELEASE RATE

The quantity measuring the material resistance against transverse cracking is the critical energy release rate, G_c. The energy release rate, G, for a given applied stress and crack spacing can be determined by the present singular finite element method. If $G < G_c$, the flaw will remain stationary. Conversely, the flaw grows when $G \geqslant G_c$.

Based on linear elastic fracture mechanics, G_c can be determined as a function of flaw size from the simple tension test of a transverse ply. Note that in this case the flaw on the edge is the most critical location. However, when the transverse ply is constrained by outer longitudinal plies, the most critical position for a flaw is at the center of the ply. G_c may be obtained as follows:

$$G_c = \frac{(1.12\sigma_t \sqrt{\pi a})^2}{E_t} = 0.883a \quad (\text{MN m}^{-1}) \tag{15}$$

where the multiplier 1.12 accounts for the stress intensity magnification of an edge crack; σ_t and E_t are the tensile strength and Young's modulus of the transverse ply and are found to be equal to 56 MPa and 14 GPa, respectively, in Bailey et al. (1979); and a is the flaw size.

In general, the flaw size is very small compared to the dimension of a transverse ply. Therefore, the calculated G is proportional to a. From eqn (15), G_c is also proportional to a: It follows that the numerical predictions obtained in the analysis will not be influenced by the value of a.

5. DETERMINATION OF THE CRITICAL APPLIED STRESS

The method used to determine σ_c, the critical value of the applied far field stress at which crack propagation occurs, is as follows. The energy release rate, G, is a function of the applied stress for a given critical flaw location, ply properties, and the geometry of the laminate. Also, G is a function of ε_0, a constant strain in the z-direction due to the generalized plane strain condition. Therefore, we have two unknowns, σ_c and ε_0, to be determined for flaw growth. Under the action of an applied unit stress, we can obtain A_s, B_s, and P_s, where
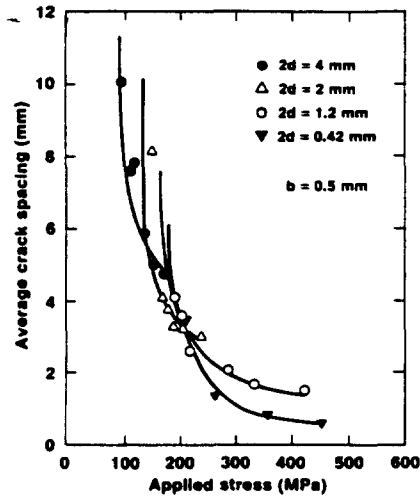
Fig. 4. Experimentally observed average crack spacing as a function of applied stress for specimens with different transverse ply thicknesses.

A and B are defined in eqns (9) and (10), respectively, and P is the total force in the z-direction due to the generalized plane strain constraint. Similarly, A_e, B_e and P_e can be obtained from the model response to a unit value of z-direction strain, ε_0.

In addition to mechanical loading, thermal effects must also be considered. In this study, the laminates are tested at room temperature, which is 125°C lower than the curing temperature. The present model is also used to obtain A_t, B_t and P_t due to thermal effects. Using the condition that the total force in the z-direction should be equal to zero, i.e.

$$\sigma_c P_s + \varepsilon_0 P_e + P_t = 0, \tag{16}$$

and the condition that $G = G_c$ at the onset of crack growth, i.e.

$$\frac{\pi}{4}(\sigma_c A_s + \varepsilon_0 A_e + A_t)(\sigma_c B_s + \varepsilon_0 B_e + B_t) = G_c, \tag{17}$$

we can solve for the two unknowns, σ_c and ε_0. Thus, given a prescribed crack spacing, the critical applied stress to cause crack growth can be determined.

6. NUMERICAL RESULTS AND DISCUSSION

The experimental results shown in Fig. 4 were obtained by Parvizi and Bailey (1978) for $[0/90]_s$ laminates with $2d = 0.42-4$ mm and $b = 0.5$ mm. These experimental data may be categorized into three stages, initiation, multiplication and saturation. The saturation of transverse cracks is also called the characteristic damage state by Reifsnider (1977). Numerical predictions from the present model are compared with the experimental results in these three stages as the applied stress increases.

6.1. Initiation of transverse cracks

It can be seen from Fig. 4 that there exists a particular stress threshold below which cracks do not occur. When the applied stress equals the stress threshold, cracks extend across the transverse ply and terminate at the outside longitudinal plies. The threshold stress (or strain) can be obtained from the present model. Consider a transverse flaw at the center of the laminate; only a representative section needs to be modeled due to symmetry.
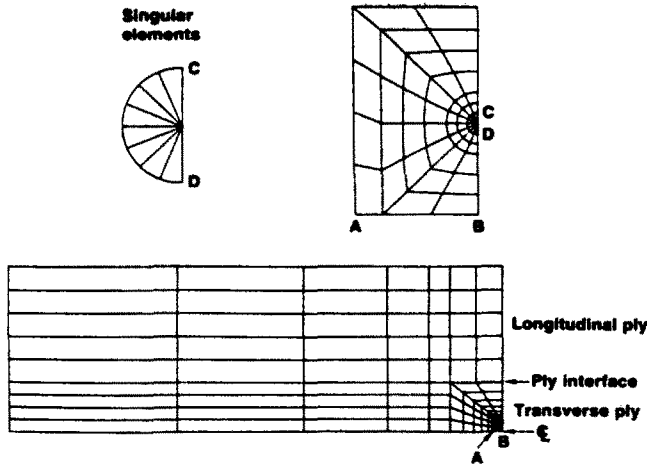
Fig. 5. Overall and local finite element mesh arrangements for modeling crack initiation.

As shown in Fig. 5, eight singular elements of identical size and shape are used. These special singular elements with a -0.5 stress singularity are embedded in the mesh of eight-node quasi-three-dimensional isoparametric elements.

The numerical predictions of threshold strain are shown in Fig. 6, both with and without thermal effects. It can be seen that the results without thermal effects are very close to a constant which may be obtained from $1.12\sqrt{2}\,\sigma_t/E_t = 0.634\%$. When thermal effects are considered, the influence of transverse ply thickness becomes more pronounced. As the thickness of the transverse ply increases, the result approaches the same constant. It should be noted that for the thickness of the transverse ply considered in this paper, the process is controlled by transverse cracking. However, for a very thin transverse ply, the process is dominated by longitudinal cracking as discussed in Dvorak and Laws (1987).

6.2. Multiplication of transverse cracks

It can be seen from experiments that subsequent cracks are introduced by increasing the applied stress. Assuming that all subsequent cracks are evenly spaced, a representative section may be considered, due to symmetry. A typical finite element mesh is shown in Fig. 7. This mesh is similar to the mesh in Fig. 5, with the exception of the additional crack between the two points E and F. Eight singular elements with the δ_1 stress singularity are placed around the crack tip (point E).

Consider a laminate with an even crack spacing, S (Fig. 7). As the applied stress reaches σ_c, the crack spacing will reduce to $S/2$. Therefore, by connecting the points (σ_c, S) for all crack spacing, the upper bound solution can be obtained. Similarly, the lower bound solution can be obtained by connecting the points $(\sigma_c, S/2)$ for all crack spacing. The numerical predictions are compared with experimental data for $2d = 0.42$, 1.2, 2 and 4 mm as shown in Figs 8-11, respectively.
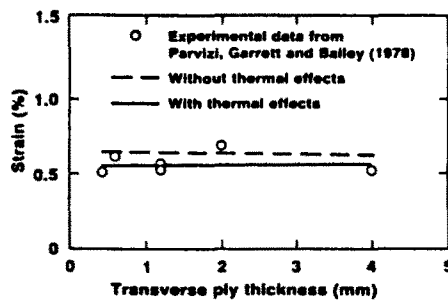

Fig. 6. Comprison of theoretical predictions with experimental data for initiation of transverse cracks in [0/90], laminate.
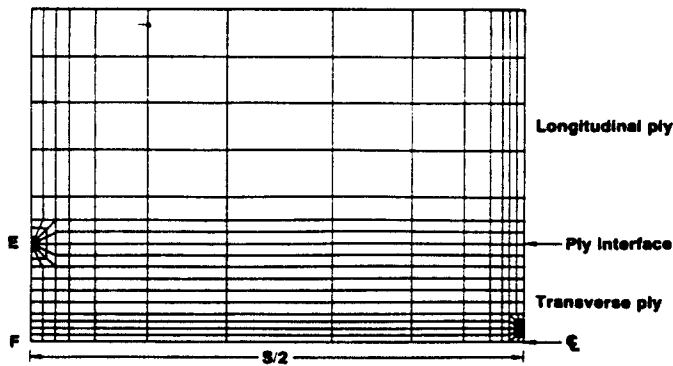
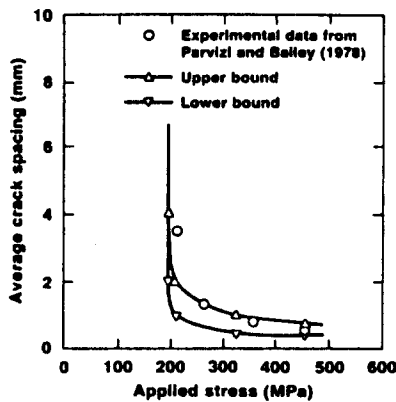Fig. 7. Overall finite element mesh arrangement for modeling crack multiplication and crack saturation.

Fig. 8. Comparison of theoretical predictions with experimental data for multiplication of transverse cracks in [0/90], laminate with $2d = 0.42$ mm
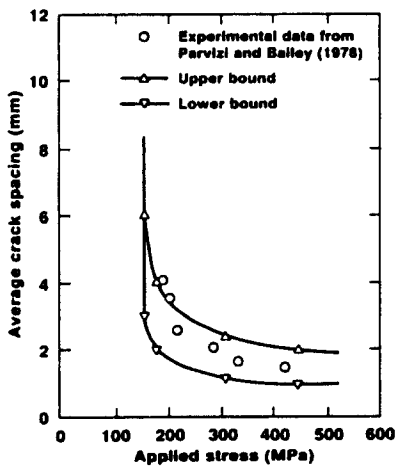

Fig. 9. Comparison of theoretical predictions with experimental data for multiplication of transverse cracks in [0/90], laminate with $2d = 1.2$ mm.

Note that for large values of applied stress, the experimental data are bounded by these two curves. In the initial stage of multiple cracking in the laminate with $2d = 0.42$, 1.2 and 2 mm, lower applied stresses are predicted than experimentally observed. This may be due to the fact that the cracks are not evenly distributed at the onset of crack multiplication. Also note that for the laminate with $2d = 4$ mm, delamination between transverse and longitudinal plies was observed by Parvizi et al. (1978). More discrepancy is expected when
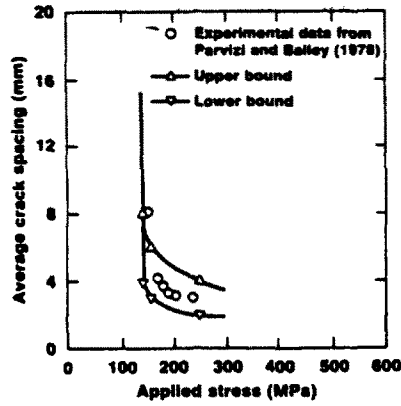
Fig. 10. Comparison of theoretical predictions with experimental data for multiplication of transverse cracks in [0/90], laminate with $2d = 2$ mm.
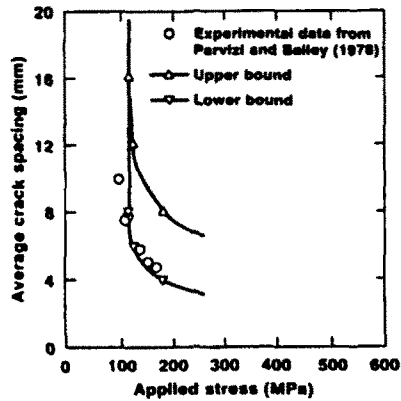

Fig. 11. Comparison of theoretical predictions with experimental data for multiplication of transverse cracks in [0/90], laminate with $2d = 4$ mm.

$2d = 4$ mm, since the interaction of delamination and transverse cracking is not considered in the present analysis.

6.3. Saturation of transverse cracks

From the observation of the laminate behavior with $2d = 0.42$ and 1.2 mm in Fig. 4, there seems to be a state of crack saturation, where the strength of the laminate is not exceeded during crack multiplication. In this stage, the thermal effects can be neglected, since the influence of the thermal effects is very small as compared with the effect of the applied stress, σ. It can be shown that G is proportional to σ^2, and will reduce as the crack spacing reduces. Therefore, the saturation crack spacing can be determined by letting $G = 0$ at the flaw tip, such that no flaw growth can occur for any value of σ. The comparison of numerical predictions and experimental results is shown in Fig. 12. Conservative predictions are obtained by the analysis.
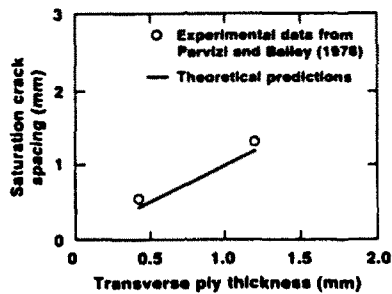

Fig. 12. Comparison of theoretical predictions with experimental data for saturation of transverse cracks in [0.90], laminate.

7. CONCLUSIONS

The fundamental nature of the stress singularity at the interface tip of the transverse crack in a [0/90]$_s$ laminate was examined. An advanced finite element method employing special singular elements containing an exact stress singularity has been used to study the fracture mechanisms of multiple transverse cracking in composite laminates. Close agreement between the numerical predictions and experimental results was obtained.

In this study, it was observed that the energy release rate at the flaw tip is proportional to the flaw size, a, since the thickness of a transverse ply is much larger than a. In some cases, it may not be true when a is of the same order as the thickness of transverse ply. Nevertheless, the present method can still be used if the exact values of G_c and a can be obtained from experiments. Furthermore, the interaction of delamination and transverse cracking was not considered in the analysis. This may be a good subject for further research.

REFERENCES

Bailey, J. E., Curtis, P. T. and Parvizi, A. (1979).On the transverse cracking and longitudinal splitting behavior of glass and carbon fiber reinforced epoxy cross ply laminates and the effect of Poisson and thermally generated strain. *Proc. R. Soc. Lond. A.* **366**, 599–623.
Comninou, M. (1977). The interface crack. *ASME J. Appl. Mech.* **44**, 631–636.
Crossman, F. W., Warren, W. J., Wang, A. S. D. and Law, G. E., Jr. (1980). Initiation and growth of transverse cracks and edge delamination in composite laminates—Part 2. Experimental correlation. *J. Composite Materials Supplement* **14**, 88–108.
Dvorak, G. J. and Laws, N. (1987). Analysis of progressive matrix cracking in composite laminates—II. First ply failure. *J. Composite Materials* **21**, 309–329.
Gradshteyn, I. S. and Ryzhik, I. M. (1980). *Table of Integrals, Series, and Products*, p. 948. Academic Press, Florida.
Highsmith, A. L. and Reifsnider, K. L. (1982). Stiffness-reduction mechanisms in composite laminates. In *Damage in Composite Materials* (edited by K. L. Reifsnider), pp. 103–117. ASTM STP775.
Irwin, G. R. (1957). Analysis of stresses and strains near the end of a crack traversing a plate. *J. Appl. Mech.* **24**, 361–364.
Lekhnitskii, S. G. (1963). *Theory of Elasticity of an Anistropic Elastic Body*. Holden-Day, San Francisco, CA.
Parvizi, A. and Bailey, J. E. (1978). On multiple transverse cracking in glass fiber epoxy cross-ply laminates. *J. Materials Sci.* **13**, 2131–2136.
Parvizi, A., Garrett, K. W. and Bailey, J. E. (1978). Constrained cracking in glass fiber-reinforced epoxy cross-ply laminates. *J. Materials Sci.* **13**, 195–201.
Reifsnider, K. L., (1977). Some fundamental aspects of the fatigue and fracture response of composite materials. *Proc., 14th Annual Society of Engineering Science Meeting*, Lehigh University, Bethlehem, PA.
Stern, M. (1979). Families of consistent conforming elements with singular derivative fields. *Int. J. Numer. Meth. Engng* **14**, 409–421.
Ting, T. C. T. and Chou, S. C. (1981). Edge singularities in anisotropic composites. *Int. J. Solids Structures* **17**, 1057–1068.
Wang, A. S. D. (1984). Fracture mechanics of sublaminate cracks in composite materials. *Composites Technology Rev.* **6**, 45–62.
Wang, A. S. D. and Crossman, F. W. (1980). Initiation and growth of transverse cracks and edge delamination in composite laminates—Part 1 An energy method. *J. Composite Materials Supplement* **14**, 71–87.
Wang, S. S. and Choi, I. (1982). Boundary-layer effects in composite laminates. *J. Appl. Mech.* **49**, 541–560.
Wang, S. S. and Choi, I. (1984). The mechanics of delamination in fiber-reinforced composite materials. *ASME J. Appl. Mech.* pp. 83–133.
Yeh, J. R. (1988). Fracture mechanics of delamination in ARALL laminates. *Engng Fracture Mech.* **30**, 827–837.
Yeh, J. R. and Tadjbakhsh, I. G. (1986). Stress singularity in composite laminates by finite element method. *J. Composite Materials* **20**, 347–364.
Zwiers, R. I., Ting, T. C. T. and Spilker, R. L. (1982). On the logarithmic singularity of free-edge stress in laminated composites under uniform extension. *J. Appl. Mech.* **49**, 561–569.

APPENDIX: SHAPE FUNCTIONS $[N_i(\rho, \xi; \delta)]$ FOR THE SINGULAR ELEMENT

Corresponding to the order of stress singularity, δ, the shape function in local triangular polar coordinates, (ρ, ξ) for the six-node conforming singular element is shown in Stern (1979) to have the following expressions:

$$[N_i] = [N_1 \mathbf{I}, N_2 \mathbf{I}, \dots, N_6 \mathbf{I}]$$ (A1)

where

$$N_1 = 1 + \frac{2 - 2^{-\delta}}{2^{-\delta} - 1}\rho - \frac{1}{2^{-\delta} - 1}\rho^{\delta + 1}$$ (A2)

$$N_2 = -\frac{2}{2^{-\delta} - 1}(1 - \xi)\rho + \frac{2}{2^{-\delta} - 1}(1 - \xi)\rho^{\delta + 1}$$ (A3)

$$N_3 = \frac{2^{-\delta}}{2^{-\delta}-1}(1-\xi)\rho - (1-\xi)\left(\frac{1}{2^{-\delta}-1}+2\xi\right)\rho^{\delta+1} \tag{A4}$$

$$N_4 = 4\xi(1-\xi)\rho^{\delta+1} \tag{A5}$$

$$N_5 = \frac{2^{-\delta}}{2^{-\delta}-1}\xi\rho - \left[\frac{1}{2^{-\delta}-1}+2(1-\xi)\right]\xi\rho^{\delta+1} \tag{A6}$$

$$N_6 = -\frac{2}{2^{-\delta}-1}\xi\rho + \frac{2}{2^{-\delta}-1}\xi\rho^{\delta+1} \tag{A7}$$

and I is the 3×3 identity matrix.

The local coordinates, ρ and ξ, are related to the global coordinates by:

$$\xi = \frac{(x_3-x_1)\tan\theta - (y_3-y_1)}{(y_5-y_3)-(x_5-x_3)\tan\theta} \tag{A8}$$

$$\rho = r/f(\xi) \tag{A9}$$

where

$$f(\xi) = \{(x_3-x_1)^2 + (y_3-y_1)^2 + 2\xi[(x_3-x_1)(x_5-x_3)+(y_3-y_1)(y_5-y_3)] + \xi^2[(x_5-x_3)^2+(y_5-y_3)^2]\}^{1/2}. \tag{A10}$$